Available online at www.sciencedirect.com
ScienceDirect
Ceramics International 37 (2011) 2275–2280
CERAMICS INTERNATIONAL
www.elsevier.com/locate/ceramint

Improving degradation rate and apatite formation ability of nanostructure forsterite

F. Tavangarian *, R. Emadi

Department of Materials Engineering, Isfahan University of Technology, Isfahan 84156-83111, Iran

Received 19 January 2011; received in revised form 10 March 2011; accepted 11 March 2011
Available online 23 March 2011

Abstract

Although micron size forsterite is biocompatible, the degradation rate of this ceramic is extremely low, and the apatite formation ability is poor as well. In this study, the influence of nanostructure and the degree of crystallinity on the apatite formation ability and degradation rate were investigated. Forsterite was synthesized by 5 h of milling of talc and magnesium carbonate and subsequent annealing at 1000 °C in the presence of chloride ion. To investigate the in vitro bioactivity and degradability, the prepared forsterite powder was pressed in the form of tablets and then immersed in simulated body fluid (SBF) and Ringer's solution, respectively. The results showed that nanostructure forsterite powder with crystallite size of about 20 nm was bioactive and released magnesium ions in the SBF solution. With increasing crystallinity degree of nanostructure forsterite, the apatite formation ability and degradation rate decreased.

Keywords: A. Milling; E. Biomedical applications

1. Introduction

Many studies have been focused on finding new biomaterials well-matched with the natural bone from the mechanical properties perspective. Hydroxyapatite is one of the most important bioceramics due to its high bioactivity and osteoconductivity properties. However, the orthopedic applications of hydroxyapatite ceramics have been limited as a result of the low fracture toughness and inappropriate mechanical properties [1–4].

Magnesium and silicon elements play crucial roles in human body. Previous investigations showed that silicon is an essential element in skeletal development. Carlisle [5–7] studied the effect of the lack of silicon on the bone growth and the influence of silicon on osteoblasts growth. The findings showed that silicon (more than 5 wt.%) was uniquely localized in the active growth areas in the bones of young rats (when the Ca/P ratio was 0.7) and involved in the early stage of bone calcification in physiological conditions. Similar studies by Schwarz and Milne [8,9] showed that the growth rate of rats was increased by adding silicon to their diets. They also showed that silicon deficiency in rats resulted in skull deformations.

Moreover, magnesium is undoubtedly one of the most important elements in human body. It is closely associated with mineralization of calcined tissues and indirectly influences mineral metabolism [10,11]. It also affects insulin secretion which participates in the regulation of bone growth [12,13].

Recently, forsterite (Mg_2SiO_4) has been introduced as a possible candidate for load bearing applications. Although it has a better bending strength and fracture toughness than those of commercially available hydroxyapatite ceramics, the degradation rate of forsterite ceramic is tremendously low, and the apatite formation ability is poor as well [14]. The aim of the present work was to investigate and optimize the in vitro apatite formation ability and degradability rate of nanostructure forsterite ceramic as opposed to previous studies. The results of this paper can be used for further researches and it would promote the possibility of usages of nanostructure forsterite ceramic in tissue engineering.

2. Experimental procedures

2.1. Preparation of samples

In this study, talc ($Mg_3Si_4O_{10}(OH)_2$) (98% purity, Merck), magnesium carbonate ($MgCO_3$) (98% purity, Merck) and ammonium chloride (NH_4Cl) (98% purity, Merck) were used as

* Corresponding author. Tel.: +98 311 3915725; fax: +98 311 3912752.
E-mail address: f_tavangarian@yahoo.com (F. Tavangarian).

0272-8842/$36.00
doi:10.1016/j.ceramint.2011.03.022

initial powders. The nanostructure forsterite powder was synthesized according to our previous study [15] in which $MgCO_3$ and talc powders were mixed at a molar ratio of 5:1 to obtain a stoichiometric forsterite structure. The powder mixtures were then milled for 5 h in a planetary ball mill (Fritsch P7 type) under ambient conditions. The ball-to-powder weight ratio was 10:1 and the rotational speed of the main disc was set at 500 rpm. NH_4Cl powder was added to the ball milled mixture and the mixture (containing NH_4Cl) thus obtained were milled for 5 min. The molar ratio of $MgCO_3$:talc:NH_4Cl powders was set to 5:1:3. Annealing of this powder was carried out at 1000 °C for 2 min and 1 h.

2.2. In vitro experiments

This part of the study was carried out using the standard in vitro procedure described in Kokubo and Takadama [16]. The obtained forsterite powders were uniaxially pressed at 500 MPa to form pellets with 12 mm in diameter and 12 mm long. These prepared bulk samples were then soaked in 70 ml simulated body fluid (SBF) (pH 7.40) at 37 °C for 1, 2, 4, 7, 14, 21, and 28 days. After soaking, the samples were dried at 100 °C for 1 day. To evaluate the degradation rate, the prepared bulk samples were soaked in 70 ml Ringer's solution (pH 7.40) at 37 °C in a shaking water bath for 1, 2, 4, 7, 14, 21, and 28 days without refreshing the soaking medium. After soaking, the samples were dried at 100 °C for 1 day, and the final weight of each sample was accurately measured. The weight loss was expressed as a percentage of the initial weight.

2.3. Characterization of samples

The functional groups on the surface of the samples soaked in SBF were investigated by Fourier transform infrared (FT-IR) spectroscopy analysis (Bomem, MB 100). The spectrum was recorded in the 4000–400 cm^{-1} region with a resolution of 2 cm^{-1}. The surface morphology of specimens was observed by scanning electron microscopy (SEM) (Seron, AIS2100, at an acceleration voltage of 20 kV) coupled with energy dispersive spectrometer (EDS). The ability of in vitro Ca–P formation or Ca–P induction was semi-quantitatively compared by SEM examinations. The concentration of Ca and Mg ions of the SBF after soaking were determined by atomic absorption spectrometer (AAS; Perkin Elmer, 2380), and the changes in the pH of SBF were also measured at predetermined time intervals (0–28 days) using an electrolyte-type pH meter.

3. Results and discussion

3.1. Phase structure analysis

Fig. 1a and b shows the structure of forsterite powders obtained after 5 h of milling with subsequent annealing at 1000 °C for 2 and 60 min in the presence of chloride ion, respectively. All the XRD peaks are correspond to the characteristic peaks of forsterite structure. As can be seen, with increasing the annealing time from 2 to 60 min, the intensity of XRD peaks increased while their width decreased. This would be attributed to the larger crystallite size and a higher crystallinity of sample annealed for the longer time [15]. The crystallite size of the forsterite powder obtained after 2 and 60 min annealing at 1000 °C was about 20 and 31 nm, respectively [15]. With increasing the holding time at elevate temperature, the phenomenon of grain growth occurred, which resulted in the higher crystallite size.

3.2. In vitro bioactivity evaluation

To evaluate the bioactivity and degradation rate of obtained nanostructure forsterite powders, two mixtures were selected. The first mixture, designated as F1, was prepared from milling of talc and magnesium carbonate for 5 h with subsequent annealing at 1000 °C for 1 h in the presence of chloride ion. The bioactivity of this sample was evaluated in our previous study [17], but for comparison purposes we present some of those results. To assess the effects of crystallinity on the degradation rate and apatite formation ability on the surface of prepared forsterite ceramics, the second mixture was prepared from milling of talc and magnesium carbonate for 5 h with subsequent annealing at 1000 °C for 2 min in the presence of chloride ion. This was designated as F2. Fig. 2a and b shows the infrared spectra of F1 and F2 specimens after soaking in SBF for various periods of time, respectively. In Fig. 2a, the infrared spectra of F1 sample before immersion in SBF corresponded to the characteristic bands of forsterite. The bands related to the characteristic bands of forsterite appeared in the range of 1100–800 cm^{-1} (SiO_4 stretching), 650–500 cm^{-1} (SiO_4 bending), and at 475 cm^{-1} (MgO_6 modes). These results substantiated the formation of forsterite as shown in the XRD pattern of this sample (Fig. 1b). The position of FTIR bands of the prepared forsterite agreed with the results reported in previous studies [18]. With increasing the immersion time of the F1 specimens, new absorption bands related to O–H, C–O, and P–O were observed. The bands at 3500 and 1621 cm^{-1} belonged to hydroxyl groups in the hydroxyapatite. Those bands at 1462 and 1420 cm^{-1} fit with bands in carbonate groups of apatite structure [17]. The low intense bands noticed at about

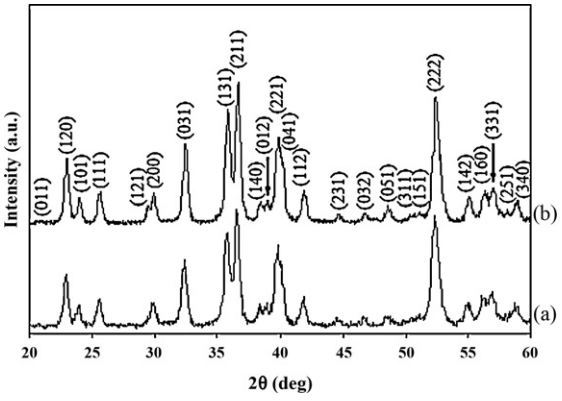

Fig. 1. XRD patterns of obtained forsterite powders after 5 h milling of initial materials with subsequent annealing at 1000 °C for (a) 2 min and (b) 1 h in the presence of chloride ion.

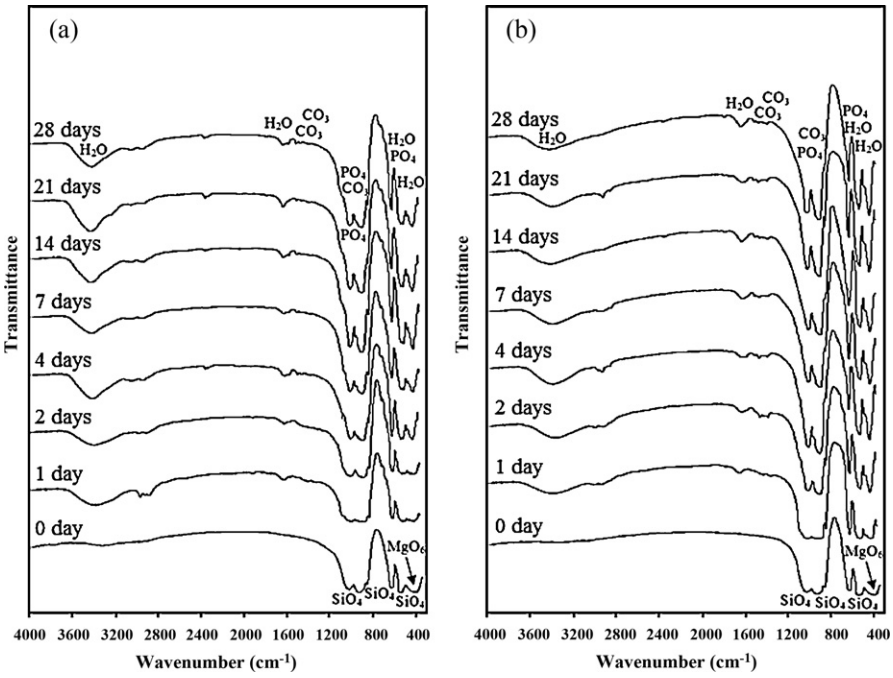

Fig. 2. FTIR spectra of (a) F1 and (b) F2 samples which were soaked in SBF for various periods of time.

2900 cm^{-1} may be attributed to H–C–O functional groups [20]. Furthermore, bands related to phosphate groups were situated in the range of 1100–1000, and 550–600 cm^{-1}. These three bands are the characteristic bands of apatite crystals which suggest the formation of apatite on the surface layer of forsterite samples after soaking in SBF [19]. As can be seen, with increasing the soaking time the intensity of O–H, C–O, and P–O absorption bands gradually increased as a result of formation of higher amount of hydroxy-carbonate apatite (HCA) on the surface of forsterite samples [17].

Fig. 2b shows the FTIR spectra of F2 after soaking in the SBF for various periods of time. With increasing the soaking time the intensity of FTIR bands got stronger, which may be related to the precipitation of HCA on the surfaces of the forsterite specimens. However, in comparison with F1 samples (Fig. 2a), the FTIR absorption peaks of F2 samples (Fig. 2b) were stronger in corresponding specimens due to the higher amount of HCA precipitation on the surface of the samples. These findings showed the formation of apatite on the surface of all specimens after soaking in SBF. The immersion test in SBF and formation of amorphous HCA precipitation on the surface of materials could be regarded as the prevalent test in order to determine the bioactivity of materials [16].Changes in ion concentrations and pH in the SBF solution

The AAS analysis was performed in order to determine the concentration of Mg and Ca ions in the SBF. Fig. 3a and b shows the results of AAS analysis obtained from SBF solutions of F1 and F2 specimens after different soaking times, respectively. Also, pH changes of solutions in the time span are shown. In general, increasing the pH and Mg ions and decreasing the Ca ions concentration in the SBF were the overall consequence of soaking the forsterite samples. As can be seen in Fig. 3a, most concentration changes of ions and pH of the SBF were in the first day of soaking as Mg ions concentration increased from 39 to 47 ppm, Ca ions concentration decreased from 114.8 to 76 ppm and pH of the solution increased from 7.4 to 7.68. These results revealed that the release of Mg ions from the forsterite ceramics accompanied with the deposition of Ca ions on the surface of forsterite samples. Furthermore, with increasing the soaking time in the SBF, Ca ions concentration decreased with a smooth slope, which could be ascribed to the consumption of these ions

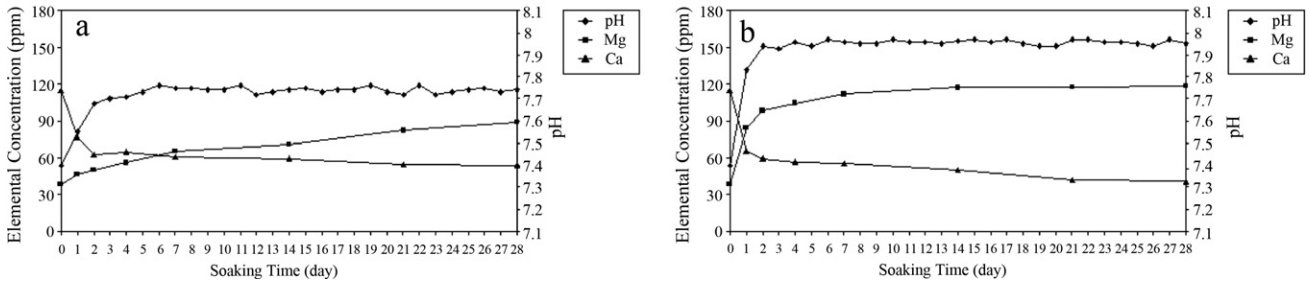

Fig. 3. Changes of Ca and Mg ions concentrations, and pH of the SBF of (a) F1 and (b) F2 samples after soaking for various periods of time.

and the formation of apatite on the surface of forsterite samples. As can be seen in Fig. 3b, the obtained results of F2 specimens showed the extreme changes in the pH, and the Ca and Mg ions concentration. After 1 day soaking, Mg ions concentration increased from 39 to 84 ppm, Ca ions concentration decreased from 114.8 to 65.6 ppm and pH of the solution increased from 7.4 to 7.83. In comparison to the results of F1 samples, F2 samples caused more changes of pH and ions concentration due to the release of higher amount of Mg ions in the SBF [21].

Considering the FTIR and AAS results, it could be suggested that F2 specimens released more ions in the SBF and therefore caused more apatite formation on the surface. As can be seen, the Mg ions concentration after 14 days tended to a fixed value as a result of saturating of the SBF with Mg ions. It could be concluded that the degradation rate of F2 samples was optimal and caused the formation of a higher amount of precipitation on the surface. Generally speaking, the formation of apatite precipitation on the bioactive surface depends on the type of ions released into the SBF and an optimal degradation rate of bioactive material.

3.4. Degradability evaluation

To determine the degradation rate, F1 and F2 samples were immersed in Ringer's solution at 37 °C up to 4 weeks. The weight loss of specimens is shown in Fig. 4. As can be seen, the weight loss of F2 samples was noticeably higher than that of F1 samples. The degradation of forsterite ceramic could provide meshes to accelerate the precipitation of HCA and increase the growth of tissues which are vital to the applications of tissue engineering.

3.5. Microstructure of the formed apatite

Fig. 5 shows the surface morphology and EDS spectra of F1 and F2 samples after immersion in SBF for various times. The surface morphology of F1 samples after immersion in SBF for 1, 14 and 28 days are shown in Figs. 5a, c, and e, respectively. As can be seen in Fig. 5a, on the surface of F1 sample after soaking in SBF for 1 day small particles could be observed. The EDS spectrum confirmed the small amount of calcium and phosphorous in this sample. After 14 days soaking of F1 sample in the SBF (Fig. 5c), some larger precipitations were recognized in the surface of the forsterite ceramic with cauliflower shape in comparison with immersed sample for 1 day (Fig. 5a). Image analysis was used to measure the particle size of precipitations. The mean deposition particle size was about 7 μm (Fig. 5c). The EDS spectrum showed that these spherical particles were composed of calcium and phosphorus. The presence of Mg and Si in the EDS spectra can be attributed to the forsterite samples. After prolonged soaking time up to 28 days, more particles were appeared on the surface of the samples. Also, some new nuclei were observed at this stage. With increasing the soaking time, the depositions grew and had a larger particle size. The mean deposition particle size was about 10 μm after 28 days soaking time. Furthermore, the EDS spectrum proved the presence of calcium and phosphorus in this specimen. The gold peak in all EDS spectra comes from the coating of the samples with Au prior to SEM measurements to avoid charging of the samples.

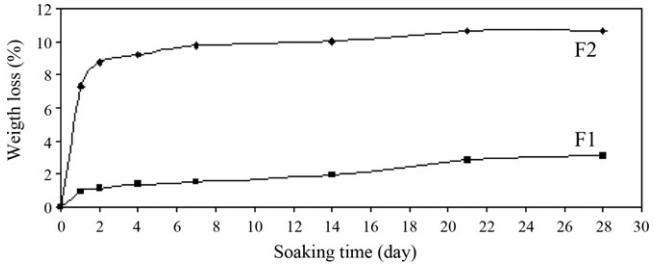

Fig. 4. The weight loss of F1 and F2 specimens in the Ringer's solution after different periods of time.

Considering the results of FTIR patterns and changes on the ions concentration in the SBF, it is expected that the formed depositions were hydroxy-carbonate apatite. Ca–P precipitations with similar morphology have been reported in previous studies [22].

In order to determine the influence of crystallinity on the apatite formation ability on the surface of the forsterite ceramics, F2 samples, which were annealed for a shorter time (2 min), were soaked in the SBF. Fig. 5b, d, and f shows the surface morphology of F2 samples after immersion in SBF for 1, 14, and 28 days, respectively. As can be seen in Fig. 5b, on the surface of F2 sample soaked in SBF for 1 day, small precipitations were detected. The EDS spectrum of this sample proved the presence of calcium and phosphorous as well. After 14 days soaking of F2 sample in SBF (Fig. 5d), the precipitation grew and got larger. The mean deposition particle size was about 11 μm. With increasing the soaking time of F2 sample up to 28 days (Fig. 5f), the surface of the forsterite ceramic was almost covered with the precipitations (with nearly spherical shape) and a higher amount of apatite (regarding the EDS results) was formed at this stage with mean precipitation particle size of about 18 μm. Comparing the obtained results of F1 (Figs. 5a, c, and e) and F2 (Figs. 5b, d, and f) specimens, it is obvious that the apatite formation ability on the surfaces of F2 samples were much higher than those of F1 samples. This could be ascribed to the optimum dissolution rate of F2 samples in comparison with F1 samples. Consequently, more nucleation sites were available for precipitation of apatite.

The bone-bonding ability of a material is often evaluated by examining the ability of apatite to form on its surface in a simulated body fluid (SBF) with ion concentrations nearly equal to those of human blood plasma. It was proposed that the examination of apatite formation on materials in SBF is useful for predicting the in vivo bone bioactivity of materials [16]. Previous results showed that although micron-sized forsterite ceramic is biocompatible, it is not bioactive [14]. Our findings suggested that nanostructure forsterite powder had apatite formation ability and was bioactive. As bioactivity in SBF is a criterion of bone bonding ability in body environment [16], it is expected that nanostructure forsterite could form bone graft. This can be ascribed to the nature of nanostructure materials. Nanostructure materials have a higher surface area to volume ratio and consequently decrease the surface stability and increase

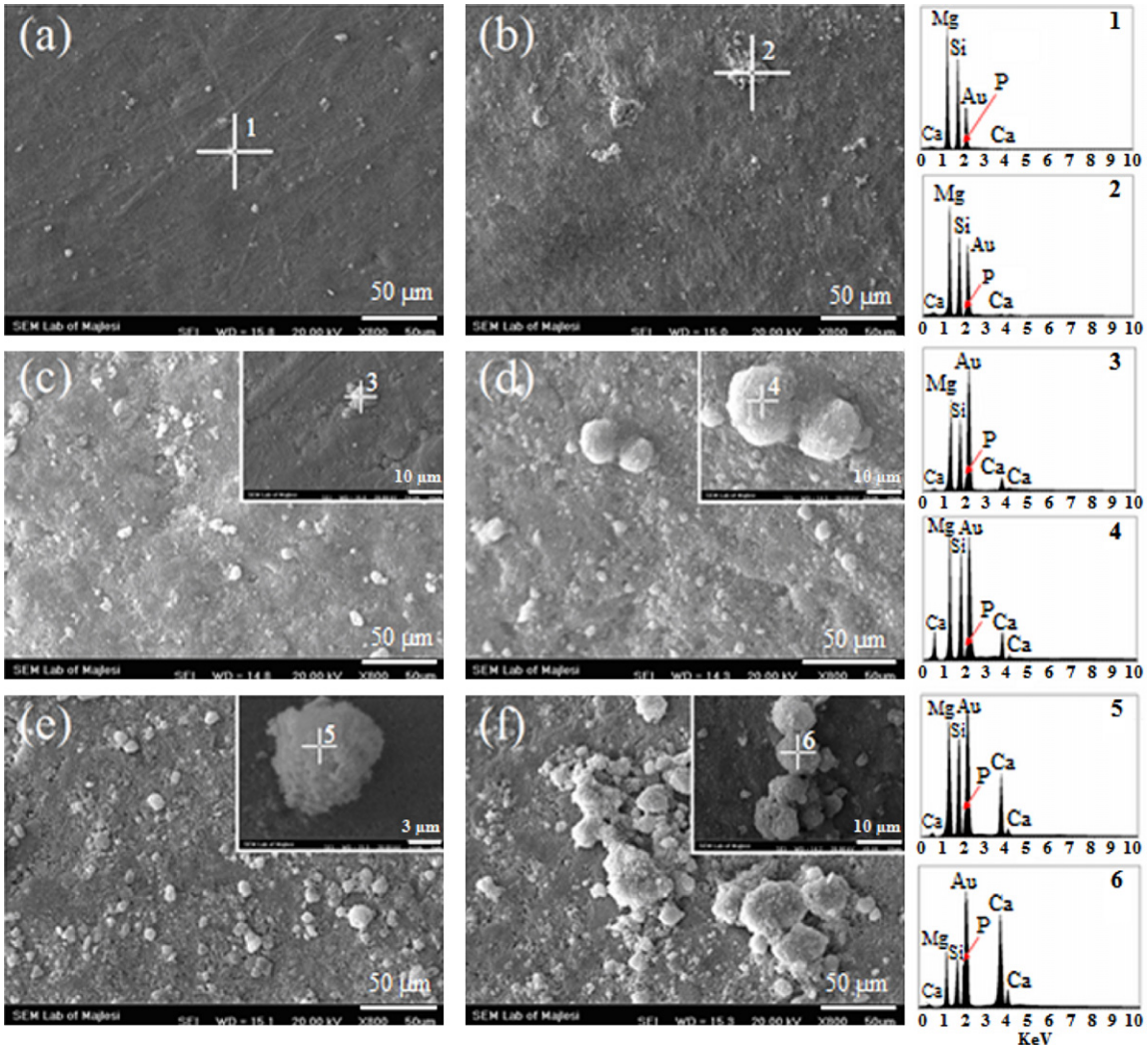

Fig. 5. SEM micrographs and EDX spectra of the surfaces of (a, c, and e) F1 and (b, d, and f) F2 samples after immersion in SBF for (a, b) 1 day, (c, d) 14 days and (e, f) 28 days.

the surface energy. As a result, the solubility of nanostructure materials is higher than that of coarse-grained materials. With dissolving of forsterite in SBF, some preferable locations were formed in the surface of the ceramic which improved the apatite formation ability of nanostructure forsterite [17]. The release of magnesium ions from the nanostructure forsterite ceramic was quantitatively estimated to support its in vitro bioresorbability (Fig. 3). Besides, as can be seen in Fig. 5, the bioactivity of nanostructure forsterite ceramic could be improved with decreasing the annealing time. Nanostructure forsterite ceramic with lower crystallinity showed better bioactivity. The results of this paper would highly influence future researches and clinical applications of nanostructure forsterite powder which has high biocompatibility, bioactivity, biodegradability, and mechanical properties in comparison with commercially available hydroxyapatite ceramics.

4. Conclusion

The behavior of nanostructure forsterite ceramic in SBF was studied to evaluate the bioactivity of prepared nanostructure forsterite. Furthermore, Ringer's solution was used to determine the degradation rate of nanostructure forsterite. AAS, FTIR and EDS results showed the presence of hydroxycarbonate apatite on the surface of forsterite ceramics. Our findings showed that prepared nanostructure forsterite ceramic, unlike micron-sized forsterite, was bioactive and had apatite formation ability. Furthermore, in the case of forsterite ceramic, lower crystallinity caused the higher bioactivity and degradation rate. In summary, nanostructure forsterite bioceramic possess improved mechanical properties, good biocompatibility, fine bioactivity and biodegradability and could be a suitable candidate for hard tissue engineering in load bearing applications.

References

[1] D. Haverty, T.K. Stanton, J.B. McMonagle, Structure and stability of hydroxyapatite: density functional calculation and Rietveld analysis, Phys. Rev. B 71 (2005) 94–103.
[2] H. Ohgushi, V.M. Goldberg, A.I. Caplan, Heterotopic osteogenesis in porous ceramics induced by marrow cells, J. Orthop. Res. 7 (1989) 568–578.

[3] M.V. Regi, J.M.G. Calbet, Calcium phosphate as substitution of bone tissues, Prog. Solid State Chem. 32 (2004) 1–31.
[4] W. Suchanek, M. Yoshimura, Processing and properties of hydroxyapatite-based biomaterials for use as hard tissue replacement implants, J. Mater. Res. 13 (1998) 94–117.
[5] E.M. Carlisle, The nutritional essentiality of silicon, Nutr. Rev. 40 (1982) 193–198.
[6] E.M. Carlisle, Biochemical and morphological changes associated with long bone abnormalities in Si deficiency, J. Nutr. 110 (1979) 1046–1055.
[7] E.M. Carlisle, Silicon as a trace nutrient, Sci. Total. Environ. 73 (1988) 95–106.
[8] K. Schwarz, A bound form of silicon in glycosaminoglycans and polyuronides, Proc. Natl. Acad. Sci. 70 (1973) 1608–1612.
[9] K. Schwartz, Growth promoting effects of Si in rats, D. Milne, Nature 4 (1972) 293–333.
[10] R.Z. LeGeros, Calcium Phosphates in Oral Biology and Medicine, in: H.M. Myers (Ed.), Monographs in Oral Sciences, Vol 15, Karger, Basel, 1991.
[11] J. Althoff, P. Quint, E.R. Krefting, H.J. Höhling, Morphological studies on the epiphyseal growth plate combined with biochemiacal and X-ray microprobe analysis, Histochemistry 74 (1982) 541–552.
[12] A.M. Pietak, J.W. Reid, M.J. Stott, M. Sayer, Silicon substitution in the calcium phosphate bioceramics, Biomaterials 28 (2007) 4023–4032.
[13] C.C. Liu, J.K. Yeh, J.F. Aloia, Magnesium directly stimulates osteoblast proliferation, J. Bone Miner. Res. 3 (1988) S104.
[14] S. Ni, L. Chou, J. Chang, Preparation and characterization of forsterite (Mg_2SiO_4) bioceramics, Ceram. Int. 33 (2007) 83–88.
[15] F. Tavangarian, R. Emadi, Effects of mechanical activation and chlorine ion on nanoparticle forsterite formation, Mater. Lett. 165 (2011) 126–129.
[16] T. Kokubo, H. Takadama, How useful is SBF in predicting in vivo bone bioactivity? Biomaterials 27 (2006) 2907–2915.
[17] F. Tavangarian, R. Emadi, Nanostructure effects on the bioactivity of forsterite bioceramic, Mater. Lett. 65 (2011) 740–743.
[18] R. Jeanolz, Infrared spectra of olivine polymorphs: alpha, beta phase and spinel, Phys. Chem. Miner. 5 (1980) 327–341.
[19] B.O. Fowler, Vibrational assignments for calcium, strontium, and barium hydroxyapatite utilizing isotopic substitution, Inorg. Chem. 13 (1974) 194–207.
[20] R. Murugan, S. Ramakrishna, K. Panduranga Rao, Nanoporous hydroxycarbonate apatite scaffold made of natural bone, Mater. Lett. 60 (2006) 2844–2847.
[21] R. Murugan, S. Ramakrishna, Aqueous mediated synthesis of bioresorbable nanocrystalline hydroxyapatite, J. Cryst. Growth 274 (2005) 209–213.
[22] Y.L. Zhang, M. Mizuno, M. Yanagisawa, H. Takadama, Bioactive behaviors of porous apatite- and wollastonite-containing glass-ceramic in two kinds of simulated body fluid, J. Mater. Res. 18 (2003) 433–441.